

# Spectral types of planetary host star candidates from OGLE III

S. Dreizler<sup>1</sup>, S. Schuh<sup>1</sup>, D. Homeier<sup>1</sup>

Institut für Astrophysik, Georg-August-Universität Göttingen, Friedrich-Hund-Platz 1, D-37077 Göttingen, Germany

received; accepted

## ABSTRACT

**Context.** The Optical Gravitational Lensing Experiment project has recently provided the OGLE III list of low-luminosity object transits from campaigns #3 and #4, reporting 40 new objects exhibiting the low-amplitude photometric eclipses expected for exoplanets. Compared to previous OGLE targets, these OGLE III candidates have been more restrictively selected and may contain low-mass planets.

**Aims.** We have secured follow-up low-resolution spectroscopy for 28 candidates out of this list (and one from the OGLE Carina fields) to obtain an independent characterization of the primary stars by spectral classification and thus better constrain the parameters of their companions.

**Methods.** We fed the constraints from these results back into an improved light curve solution. Together with the radius ratios from the transit measurements, we derived the radii of the low-luminosity companions. This allows us to examine the possible sub-stellar nature of these objects.

**Results.** Sixteen of the companions can be clearly identified as low-mass stars orbiting a main sequence primary, while 10 more objects are likely to have red giant primaries and therefore also host a stellar companion; 3 possibly have a sub-stellar nature ( $R \leq 0.15 R_{\odot}$ ).

**Conclusions.** The planetary nature of these objects should therefore be confirmed by dynamical mass determinations.

**Key words.** binaries: eclipsing - stars: low-mass - stars: brown dwarfs - stars: planetary systems

## 1. Introduction

The detection of planets outside our solar system has been a longstanding goal of astronomy. After the first detections (Wolszczan & Frail 1992; Mayor & Queloz 1995), an intensive search with various methods began (see Schneider 2001 for an overview). Out of the more than 200 currently known planets, most have been detected with Doppler-velocity measurements of the planets' (late type main sequence) host stars. With increasing precision, the application of the Doppler-method could be extended to Neptune-mass planets (e.g. Santos et al. 2004).

Meanwhile, planet detections using alternatives to the Doppler method have also been successfully applied. The first four microlensing planets have been detected (Bond et al. 2004; Udalski et al. 2005; Beaulieu et al. 2006; Gould et al. 2006), possible first direct images of extra-solar planets were published (Chauvin et al. 2004, 2005a,b; Neuhäuser et al. 2005; Biller et al. 2006), and the number of detections due to transit searches increased to fourteen (Sato et al. 2005; Bouchy et al. 2005b; McCullough et al. 2006; Bakos et al. 2006; O'Donovan et al. 2006; Collier Cameron 2006).

The transit method is of special interest, since it permits the derivation of additional planetary parameters like the radius either indirectly via the radius determination of the host star or directly via detection of the secondary eclipse as observed with the Spitzer Space Telescope (Charbonneau et al. 2005; Deming et al. 2005). If combined with a radial velocity variation measurement, the mass and mean density can be determined, allowing us to obtain constraints for the planetary structure. Furthermore, transiting systems allow us to investigate the plan-

ets' atmospheres (Charbonneau et al. 2002; Vidal-Madjar et al. 2004).

This potentially large scientific output motivated the initiation of several photometric monitoring projects to detect planetary transits. Currently, OGLE (Optical Gravitational Lensing Experiment, e.g. Udalski et al. 2002a,b,c, 2003) is the most successful one with five of the fourteen confirmed transit planets out of 137 candidates. Additional 40 transiting planetary/low-luminosity companions were announced by OGLE (Udalski et al. 2004), increasing their total number of candidates to 177. These objects were extracted from a sample of stars observed during two campaigns of several weeks of photometric monitoring between February and July 2003 (and some additional observations in 2004). In a sub-sample of 230 000 stars with a photometric accuracy better than 1.5%, these 40 candidates exhibit shallow ( $\leq 0.05$  mag), flat-bottomed eclipses in their light curves, indicating the presence of a transiting low-luminosity companion. The radii of the visible primaries and of the invisible secondaries were derived from the analyses of the light curves. Compared to previous OGLE candidates, these are more restrictively selected. The candidate list contains several (relatively) bright targets and several targets with very shallow transits. Preliminary analyses of the light curves by Udalski et al. (2004) indicate possible planets down to Neptune size. The primary and companion radius estimates, derived from the eclipse duration and the orbital period by adopting a main sequence mass-radius relation, are based on the assumption of a central passage. This can only be confirmed from light curve studies by detailed analysis of the transit shape (Seager & Mallén-Ornelas 2003; Tingley & Sackett 2005), which is difficult with the currently available photometric data.

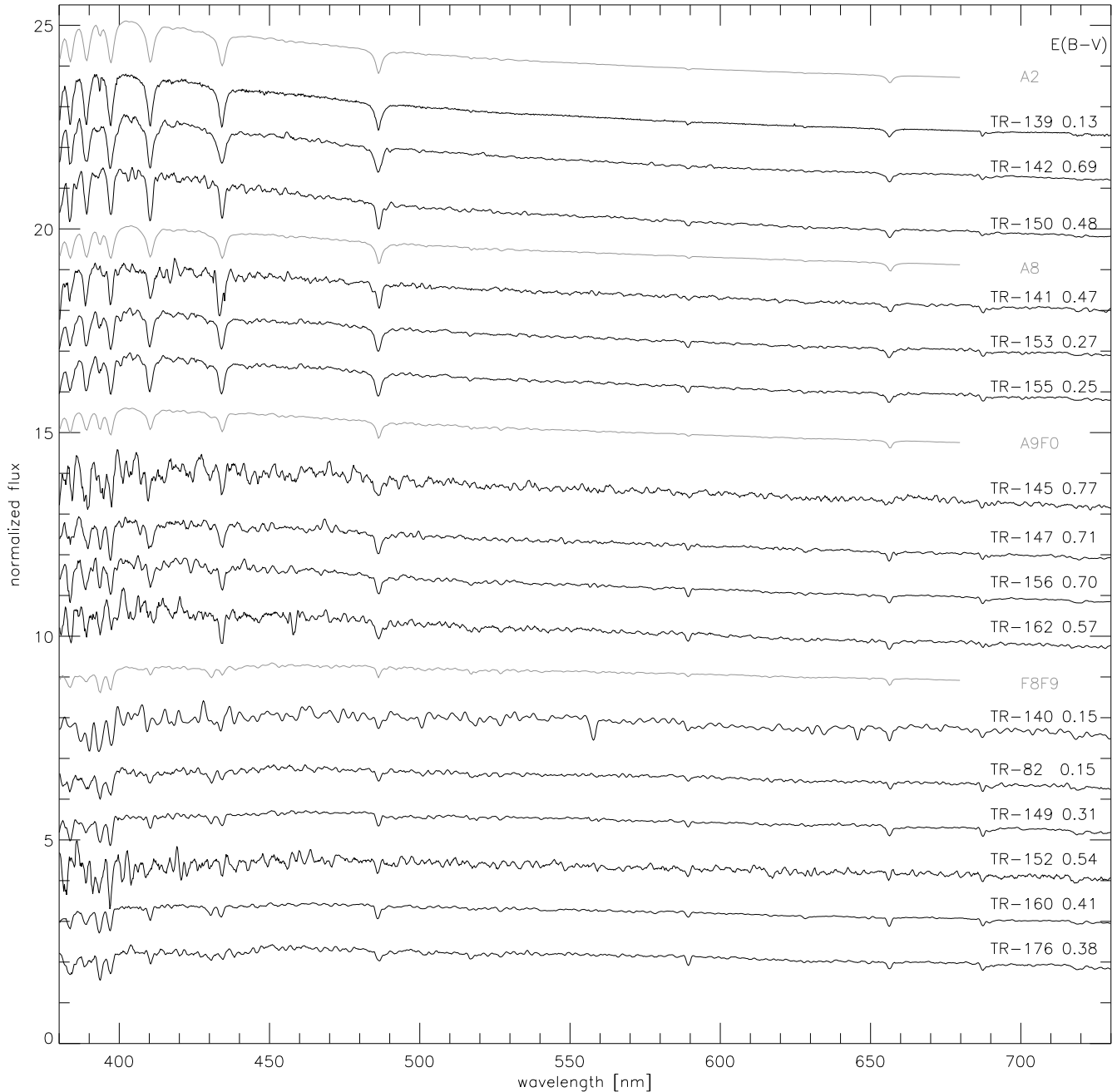


**Fig. 1.** Optical spectra of the early type target stars down to spectral type F9 together with template spectra (in grey) from Silva & Cornell (1992) and the derived reddening. See text for details.

Transit searches are a very promising method for detecting planets, even from ground-based telescopes (Gillon et al. 2005). The success of all ongoing and future transit searches depends on the rejection of false positives caused by low-mass main sequence companions, blends, and grazing eclipses. The necessity for such a pre-selection can be seen from the large fraction of blends in the sample of Konacki et al. (2003b, 4 likely blends out of 5 candidates). Based on OGLE candidate lists, several selection techniques have been used to reduce the amount of high-resolution spectroscopy for a final dynamical mass determination. Gallardo et al. (2005) use low resolution spectroscopy in combination with IR photometry in order to exclude giant primary stars and provide accurate effective temperatures and radii of the OGLE-candidates. From low resolution spectroscopy,

Heinze & Hinz (2005) have identified possible giant stars among the candidates OGLE-TR-134 through OGLE-TR-137.

Up to now, no spectroscopic information of the primaries from the latest OGLE-list (Udalski et al. 2004) has been published. The aim of this project therefore is to provide this information and to decide about the nature of these low-luminosity companions. The spectral type provides a constraint for the primary radius which, together with the transit light curve, permits a more accurate determination of the radius of the unseen companion. Using data from the SAAO 1.9 m+SpCCD, we previously weeded out many A+M-star pairs from the first OGLE list with this procedure (Dreizler et al. 2002). The remaining objects with radii suitable for sub-stellar objects can then be considered for further follow-up to obtain a dynamical mass measurement for the unseen companion from radial velocity variations.

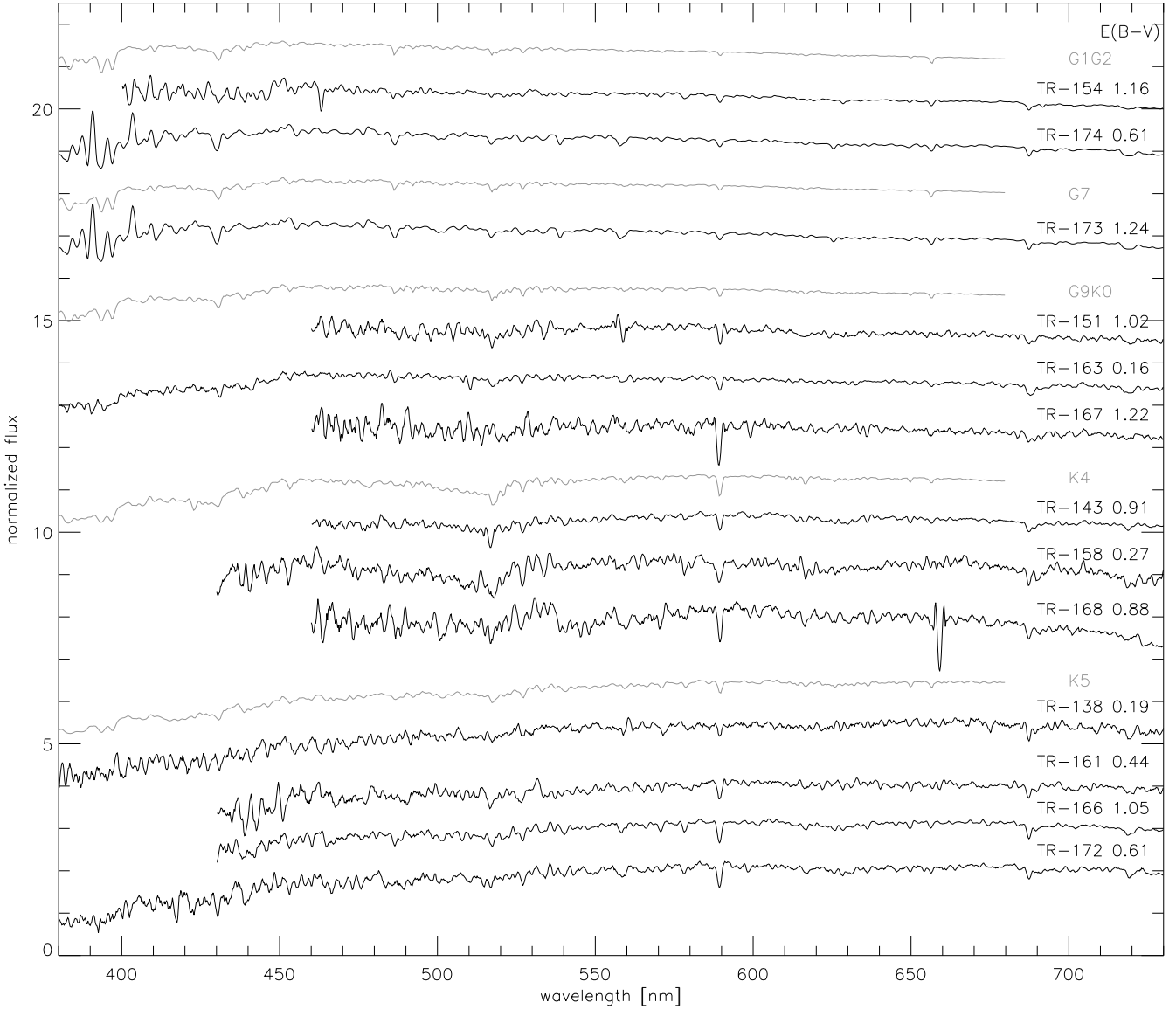


**Fig. 2.** Optical spectra of our late type target stars together with template spectra (in grey) from Silva & Cornell (1992) **and the derived reddening**. Depending on the brightness of the object as well as on the observing conditions, spectra could only be extracted in a limited spectra range. See text for details.

We describe the observations, data reduction and the determination of the spectral types of the primaries in Sect. 2, and present improved light curve solutions. The results are discussed in Sect. 3.

## 2. Observations, data reduction, and spectral types of the primary stars

### 2.1. Spectra

We selected 28 candidates from the OGLE III list of Udalski et al. (2004), with objects taken from both campaign #3 (fields at RA=11 h) and campaign #4 (fields at RA=13 h). All objects with  $m_I < 16.35$  were observed. Stars with entries in the ESO Data Archive for high-resolution spectra were given a low priority. Following the suggestion of Pont et al. (2005b), we also added OGLE-TR-82 to the target list (see Table 1).

The spectra were obtained at the SAAO 1.9 m telescope between 2005/04/26 and 2005/05/02 using the spCCD Grating

Spectrograph equipped with a  $266 \times 1798$  SITE chip. The grating 7 in combination with a slit width of  $1.5''$  provided a spectral resolution of  $5 \text{ \AA}$ , and exposure times ranged from 1800 s to 7200 s depending on the observing conditions and the brightness of the objects. Standard data reduction of these long-slit spectra was performed using IDL and included bias subtraction, flat-field correction, as well as wavelength calibration. Flux calibration was done using spectra from the standard stars EG 274 and LTT 4364. Due to the varying weather condition, the signal-to-noise ratio of the spectra varies from 10 (OGLE-TR-168) to about 200 (OGLE-TR-139). Most spectra have a signal-to-noise ratio between 30 and 50.

The spectra were compared to the spectral library of Silva & Cornell (1992) without interpolation within the library. Both observed and template spectra were normalized prior to comparison with a polynomial fit to the continuum. The quality of the match between observed and template spectrum was determined with an  $\chi^2$  test (with a reduced  $\chi^2$  ranging from 0.99 to 1.2 for the best fits) allowing us a classification better than half a

**Table 1.** Results for our program stars: Derived spectral types and radii of the primary star (columns 2, 3). The transit depth from the OGLE light curve provides the companion radius  $R_c$  (columns 4 to 5) followed by the ellipsoidal variation  $\delta I_e$ . The left hand value is derived from the OGLE light curve (“< 0.5” denotes cases where a formal fit results in amplitudes between 0.1 and 0.5 mmag), while the right hand value is from a *Nightfall* simulation of the corresponding system assuming a stellar companion (only values not in accordance with amplitudes in the observed light curves are given). *Nightfall* fits are given in columns 7 to 12 followed by our final assessment. See text for details.

#	type	$R_s/R_\odot$	$R_c/R_s$	$R_c/R_\odot$	$\delta I_e$ [mmag]	$R_s/R_\odot$	$R_c/R_\odot$	i [deg]	$R_c/R_\odot$	3 <sup>rd</sup> light [%]	$R_c/R_\odot$	cat.
	spectral type			OGLE		Nightfall fit		Nightfall fit		Nightfall fit		
82	F8F9	$1.16^{+0.1}_{-0.9}$	0.18	$0.20^{+0.01}_{-0.16}$	0.68 5.52	$0.71 \pm 0.09$	$0.10 \pm 0.03$	< 80	$0.20 \pm 0.01$	$70 \pm 10$	$0.29 \pm 0.02$	S
138	G9K0	$0.86^{+0.1}_{-0.3}$	0.12	$0.10^{+0.01}_{-0.03}$		$0.85 \pm 0.08$	$0.10 \pm 0.05$	$86 \pm 1$	$0.10 \pm 0.01$	$50 \pm 10$	$0.14 \pm 0.01$	
138	K5	$0.72^{+0.1}_{-0.1}$	0.12	$0.09^{+0.01}_{-0.01}$	0	$0.67 \pm 0.04$	$0.09 \pm 0.03$	$89 \pm 1$	$0.09 \pm 0.01$	$25 \pm 5$	$0.10 \pm 0.01$	SP
139	A2	$2.12^{+0.5}_{-1.7}$	0.17	$0.35^{+0.08}_{-0.28}$	<.5 1.28	$1.70 \pm 0.22$	$0.26 \pm 0.10$	$80 \pm 1$	$0.41 \pm 0.05$	$80 \pm 10$	$0.73 \pm 0.20$	S
140	F8F9	$1.16^{+0.1}_{-1.7}$	0.20	$0.23^{+0.01}_{-0.33}$	1.13 0.17	$0.84 \pm 0.08$	$0.17 \pm 0.05$	$83 \pm 1$	$0.42 \pm 0.02$	$80 \pm 10$	$0.85 \pm 0.40$	S
141	A8	$1.58^{+0.1}_{-1.7}$	0.13	$0.21^{+0.01}_{-0.22}$	<.5	$1.47 \pm 0.50$	$0.18 \pm 0.05$	$83 \pm 4$	$0.44 \pm 0.24$	$15 \pm 15$	$0.20 \pm 0.01$	S
142	A2	$2.12^{+0.5}_{-1.7}$	0.18	$0.37^{+0.08}_{-0.30}$	0 0.88	$1.30 \pm 0.24$	$0.18 \pm 0.05$	$80 \pm 1$	$0.51 \pm 0.06$	$90 \pm 5$	$0.87 \pm 0.13$	S
143	K4	$0.75^{+0.1}_{-0.1}$	0.07	$0.06^{+0.01}_{-0.01}$	<.5	$0.54 \pm 0.02$	$0.06 \pm 0.04$	$87 \pm 1$	$0.08 \pm 0.01$	$10 \pm 10$	$0.07 \pm 0.01$	G
145	A9F0	$1.52^{+0.1}_{-1.7}$	0.13	$0.20^{+0.01}_{-0.22}$	<.5	$1.79 \pm 0.12$	$0.21 \pm 0.05$	$89 \pm 1$	$0.20 \pm 0.02$	$5 \pm 5$	$0.20 \pm 0.02$	S
147	A9F0	$1.52^{+0.1}_{-1.7}$	0.17	$0.25^{+0.01}_{-0.27}$	0	$1.57 \pm 0.35$	$0.22 \pm 0.08$	$82 \pm 5$	$0.40 \pm 0.17$	$70 \pm 20$	$0.57 \pm 0.23$	S
149	F8F9	$1.16^{+0.1}_{-0.9}$	0.15	$0.18^{+0.01}_{-0.14}$	0.87 0	$1.00 \pm 0.07$	$0.16 \pm 0.02$	$85 \pm 2$	$0.24 \pm 0.06$	$55 \pm 35$	$0.40 \pm 0.23$	S
150	A2	$2.12^{+0.5}_{-1.7}$	0.07	$0.14^{+0.03}_{-0.11}$	<.5	$1.98 \pm 0.07$	$0.13 \pm 0.10$	$83 \pm 2$	$0.13 \pm 0.01$	$70 \pm 20$	$0.28 \pm 0.11$	S
151	G9K0	$0.86^{+0.1}_{-0.3}$	0.14	$0.12^{+0.01}_{-0.04}$	0	$0.93 \pm 0.05$	$0.11 \pm 0.02$	$87 \pm 3$	$0.13 \pm 0.02$	$45 \pm 25$	$0.18 \pm 0.06$	G
152	F8F9	$1.16^{+0.1}_{-0.9}$	0.13	$0.15^{+0.01}_{-0.12}$	0	$1.52 \pm 0.13$	$0.18 \pm 0.05$	$86 \pm 3$	$0.19 \pm 0.05$	$60 \pm 10$	$0.28 \pm 0.08$	S
153	A8	$1.58^{+0.1}_{-1.7}$	0.17	$0.26^{+0.02}_{-0.28}$	0.76 0.18	$1.04 \pm 0.07$	$0.17 \pm 0.04$	$81 \pm 4$	$0.54 \pm 0.27$	$50 \pm 45$	$0.51 \pm 0.30$	S
154	G1G2	$1.05^{+0.1}_{-0.6}$	0.11	$0.11^{+0.01}_{-0.06}$	<.5	$1.23 \pm 0.08$	$0.13 \pm 0.04$	$84 \pm 3$	$0.15 \pm 0.01$	$35 \pm 35$	$0.20 \pm 0.08$	G
155	A6	$1.66^{+0.1}_{-1.7}$	0.09	$0.14^{+0.01}_{-0.15}$		$1.43 \pm 0.27$	$0.13 \pm 0.06$	$82 \pm 3$	$0.28 \pm 0.10$	$45 \pm 45$	$0.36 \pm 0.22$	
155	A8	$1.58^{+0.1}_{-1.7}$	0.09	$0.14^{+0.01}_{-0.15}$	<.5	$1.53 \pm 0.11$	$0.13 \pm 0.06$	$84 \pm 5$	$0.23 \pm 0.10$	$50 \pm 40$	$0.35 \pm 0.22$	S
156	A9F0	$1.52^{+0.1}_{-1.7}$	0.18	$0.27^{+0.01}_{-0.29}$	0	$0.84 \pm 0.08$	$0.15 \pm 0.02$	$80 \pm 3$	$0.40 \pm 0.05$	$80 \pm 10$	$0.60 \pm 0.25$	S
158	K4	$0.75^{+0.1}_{-0.1}$	0.13	$0.11^{+0.01}_{-0.01}$	0	$0.39 \pm 0.02$	$0.06 \pm 0.01$	$87 \pm 1$	$0.15 \pm 0.02$	$15 \pm 5$	$0.10 \pm 0.01$	SP:
160	F6F7	$1.24^{+0.1}_{-1.3}$	0.09	$0.11^{+0.01}_{-0.11}$		$1.39 \pm 0.21$	$0.12 \pm 0.05$	$84 \pm 3$	$0.17 \pm 0.05$	$50 \pm 20$	$0.21 \pm 0.08$	
160	F8F9	$1.16^{+0.1}_{-0.9}$	0.09	$0.10^{+0.01}_{-0.08}$	<.5	$1.12 \pm 0.09$	$0.10 \pm 0.05$	$85 \pm 2$	$0.14 \pm 0.03$	$25 \pm 20$	$0.15 \pm 0.04$	SP:
161	G9K0	$0.86^{+0.1}_{-0.3}$	0.07	$0.06^{+0.01}_{-0.02}$		$1.54 \pm 0.08$	$0.14 \pm 0.04$	$90 \pm 0$	$0.10 \pm 0.01$	$10 \pm 10$	$0.11 \pm 0.01$	
161	K5	$0.72^{+0.1}_{-0.1}$	0.07	$0.05^{+0.01}_{-0.01}$	0	$1.09 \pm 0.14$	$0.10 \pm 0.05$	$89 \pm 1$	$0.06 \pm 0.01$	$10 \pm 10$	$0.07 \pm 0.01$	G
162	A9F0	$1.52^{+0.1}_{-1.7}$	0.10	$0.15^{+0.01}_{-0.17}$	0	$1.12 \pm 0.17$	$0.10 \pm 0.04$	$81 \pm 4$	$0.20 \pm 0.05$	$50 \pm 40$	$0.31 \pm 0.17$	S
163	G7	$0.89^{+0.1}_{-0.4}$	0.18	$0.16^{+0.01}_{-0.06}$		$0.77 \pm 0.06$	$0.12 \pm 0.01$	$81 \pm 1$	$0.15 \pm 0.01$	$80 \pm 10$	$0.34 \pm 0.11$	
163	G9K0	$0.86^{+0.1}_{-0.3}$	0.18	$0.15^{+0.01}_{-0.05}$	0.5 2.22	$0.73 \pm 0.04$	$0.11 \pm 0.01$	$81 \pm 1$	$0.15 \pm 0.01$	$70 \pm 5$	$0.24 \pm 0.01$	S
166	G9K0	$0.86^{+0.1}_{-0.3}$	0.10	$0.09^{+0.01}_{-0.03}$		$1.09 \pm 0.06$	$0.11 \pm 0.03$	$90 \pm 0$	$0.10 \pm 0.01$	$25 \pm 25$	$0.13 \pm 0.02$	
166	K5	$0.72^{+0.1}_{-0.1}$	0.10	$0.07^{+0.01}_{-0.01}$	0	$0.97 \pm 0.03$	$0.10 \pm 0.04$	$90 \pm 0$	$0.07 \pm 0.01$	$25 \pm 25$	$0.09 \pm 0.01$	G
167	G9K0	$0.86^{+0.1}_{-0.3}$	0.14	$0.12^{+0.01}_{-0.04}$	0.83 0	$0.81 \pm 0.04$	$0.11 \pm 0.03$	$88 \pm 1$	$0.14 \pm 0.02$	$40 \pm 35$	$0.18 \pm 0.06$	G
168	K4	$0.75^{+0.1}_{-0.1}$	0.11	$0.08^{+0.01}_{-0.04}$	0	$0.80 \pm 0.03$	$0.10 \pm 0.03$	$90 \pm 0$	$0.09 \pm 0.01$	$40 \pm 30$	$0.13 \pm 0.03$	G
172	G9K0	$0.86^{+0.1}_{-0.3}$	0.07	$0.06^{+0.01}_{-0.02}$		$0.99 \pm 0.05$	$0.08 \pm 0.04$	$87 \pm 2$	$0.09 \pm 0.01$	$50 \pm 5$	$0.12 \pm 0.02$	
172	K5	$0.72^{+0.1}_{-0.1}$	0.07	$0.05^{+0.01}_{-0.01}$	0.57 0.3	$0.90 \pm 0.04$	$0.07 \pm 0.03$	$89 \pm 1$	$0.06 \pm 0.01$	$55 \pm 25$	$0.09 \pm 0.03$	G
173	G7	$0.89^{+0.1}_{-0.4}$	0.13	$0.12^{+0.01}_{-0.05}$	0	$0.69 \pm 0.07$	$0.09 \pm 0.03$	$83 \pm 2$	$0.19 \pm 0.06$	$35 \pm 35$	$0.13 \pm 0.07$	G
174	G1F2	$1.05^{+0.1}_{-0.9}$	0.12	$0.13^{+0.01}_{-0.13}$	<.5	$0.79 \pm 0.19$	$0.08 \pm 0.05$	$83 \pm 2$	$0.19 \pm 0.04$	$70 \pm 20$	$0.29 \pm 0.10$	G
176	F8F9	$1.16^{+0.1}_{-0.9}$	0.14	$0.16^{+0.01}_{-0.16}$	<.5	$1.26 \pm 0.14$	$0.16 \pm 0.02$	$84 \pm 3$	$0.22 \pm 0.06$	$35 \pm 35$	$0.28 \pm 0.10$	S

spectral class, sufficient for our further analysis. For target stars with multiple spectra we obtained spectral classifications within this error limit. Due to the absence of sufficiently strong features for our spectral resolution and due to the low signal-to-noise a

discrimination between late G and mid K was difficult so that we list the solutions for both possible classifications.

In a first step, we restricted the the classification to luminosity class V, because a discrimination between different luminosity classes is too uncertain from our spectra. We also determined

the interstellar reddening assuming  $R_V=3.1$  with the IDL routine *ccm\_unred*. This spectral classifications of all objects and the derived reddenings are displayed in Figs. 1 and 2 with the inverse polynomial function that we used to normalize the template spectrum of the corresponding spectral type applied to the observed spectrum. The presence of the companion could not be detected from our data, neither from double lined spectra nor from the flux distribution.

In a second step we checked our restriction to luminosity-class V with a procedure adapted from Gallardo et al. (2005). The interstellar extinction was modeled according to a simple homogeneous exponential disc for distances from 0 to 1.5 kpc using  $k_0 = 0.70$  and  $k_0 = 1.05$ . While Gallardo et al. (2005) used IR photometry, we took the I magnitudes from Udalski et al. (2004), de-reddened with the modeled extinction, and intrinsic colors corresponding to the derived spectral type taken from Ramírez (2005). We could then determine the limb-darkened angular diameter of the stars using the results of Kervella et al. (2004). The strong correlation of mass and luminosity, as well as mass and radius on the main sequence, allowed us to derive an effective temperature as a function of distance (Eq. 10 of Gallardo et al. 2005). The effective temperatures and the reddenings derived from the spectra should therefore be consistent with this curve. This is not the case for objects with extreme reddening even if we take uncertainties in the brightness, spectral class, and flux calibration with conservative error bars into account. These stars are likely to be giants, marked with *G* in the last column of Table 1. For the further evaluation, we however assume a main-sequence primary for all systems.

## 2.2. Light curves

We then used the derived spectral classes to estimate the stellar radii of the primary stars (Table 1, column 3) by interpolating the tabulated values from Cox (2000). The uncertainty range, also indicated in Table 1, is calculated from zero-age and terminal-age main-sequence models from Schaller et al. (1992) and Charbonnel et al. (1999) with solar metallicity. This reflects the spread of interferometric radius determinations from e.g. Kervella et al. (2004) for  $\alpha$  Cen A and  $\tau$  Ceti, where the former is 20% larger, the latter 10% smaller compared to the interpolated radius using the values from Cox (2000) for a G2V or G8V star, respectively. The photometric monitoring of Udalski et al. (2004) provides the brightness variation during eclipses. Assuming a negligible radiation from the secondary, a central passage in front of the primary, and no third light contribution, this brightness variation is directly proportional to the radius ratio squared. When multiplied by the primary radius it yields the radius of the secondary (Table 1, column 5). Not indicated in Table 1 are the masses for the primary star, which we derived from the tabulated values from Cox (2000), Schaller et al. (1992), and Charbonnel et al. (1999) corresponding to the radii, and for the secondary object, which were derived from evolutionary models for low-mass stars of Baraffe et al. (1998), Chabrier et al. (2002), and Baraffe et al. (2002) assuming a low-mass star companion.

Using the derived radii and masses as initial start parameters, we fitted the OGLE light curves with the close binary program *Nightfall*<sup>1</sup> written by Rainer Wichmann. Best values and uncertainties were derived from  $\chi^2$ -contours by varying the parameters. First, we fixed the inclination to  $90^\circ$  and fitted the radii of both components (Table 1, columns 7, 8). In a second

step, we kept the primary radius fixed at the spectroscopically-derived values and fitted the orbital inclination, as well as the secondary radius (columns 9, 10). Results generally agree with our spectroscopically-derived values (Table 1). Finally, we also investigated the possible presence of third light contribution (columns 11, 12); however, the constraints from the light curves are not very stringent in that case. The solution for the most promising candidates, i.e. with radii equal or below  $0.15 R_\odot$ , are shown together with the OGLE light curves in Fig. 3 using the values from columns 3 and 5 in Table 1.

We also investigated the ellipsoidal variation of the light curve out of the eclipses (Table 1, column 6). We estimated the  $1\sigma$  detection significance level to be about 0.3 mmag. OGLE-TR-140 shows the largest amplitude of 1.13 mmag. In this case, the ellipsoidal variation can only be explained with a shorter orbital period. Inspection of the original light curve indeed indicated a period of 1.69665 days rather than 3.3933 days of Udalski et al. (2004). From our *Nightfall* simulation for the OGLE-TR-140 system with a 1.69665 days orbital period we derived an ellipsoidal variation with an amplitude of 1.16 mmag, in agreement with the observation, while the original period would result in about a tenth of the observed amplitude. OGLE-TR-149, OGLE-TR-153, OGLE-TR-167, and OGLE-TR-172 also show lower amplitude in the simulations. As for OGLE-TR-140, a shorter period might also be acceptable from the light curve. For OGLE-TR-82, OGLE-TR-139, OGLE-TR-142, and OGLE-TR-163, the amplitude from the simulated light curves is clearly larger than from the observed one. For OGLE-TR-139 and OGLE-TR-142, twice the orbital period would bring the simulations in agreement with observations. For OGLE-TR-82, an at least a factor of three longer period is required in order to reduce the ellipsoidal variation to the observed amplitude. The significance for the period of OGLE-TR-163 is very high due to 23 transit events. If we fix the period and adjust the secondary mass in order to fit the ellipsoidal variation, a brown-dwarf companion of 20-40 Jupiter masses fits best.

## 3. Discussion

Depending on the companion radii obtained from our investigations, we defined three categories. (1) The 16 objects (including OGLE-TR-82) in category *S* have companions of stellar size, i.e. a radius larger than  $0.15 R_\odot$  for all determined values (columns 5, 8, 10, and 12 in Table 1). (2) Regardless of the analysis of the light curve, *G* classifies binaries that are likely to have a giant primary star as derived from the spectral analysis and therefore also have a main sequence companion. (3) *SP* are objects with radii compatible with either small M stars or young sub-stellar objects, i.e. a radius between 0.1 and  $0.15 R_\odot$  (3 objects). Those with one of the values above the limit of  $0.15 R_\odot$  are marked with a “.”. There are no clear planetary candidates, i.e. with radii below the stellar limit ( $0.1 R_\odot$ ).

More follow-up observations enabling a dynamical mass determination can finally confirm the nature of these objects. While objects from category *S* and *G* can be excluded from future observations aiming at planet detections, three deserve closer inspection: OGLE-TR-138, OGLE-TR-158, OGLE-TR-160, and possibly OGLE-TR-163, which either have very small stellar companions like OGLE-TR-122b (Pont et al. 2005a) or sub-stellar companions with large radii like HD 209458b.

Several of the objects analyzed here are now subject to high-resolution studies according to the ESO Data Archive. The near future will therefore shed more light on the nature of several of our program stars.

<sup>1</sup> <http://www.lsw.uni-heidelberg.de/~rwichman/Nightfall.html>

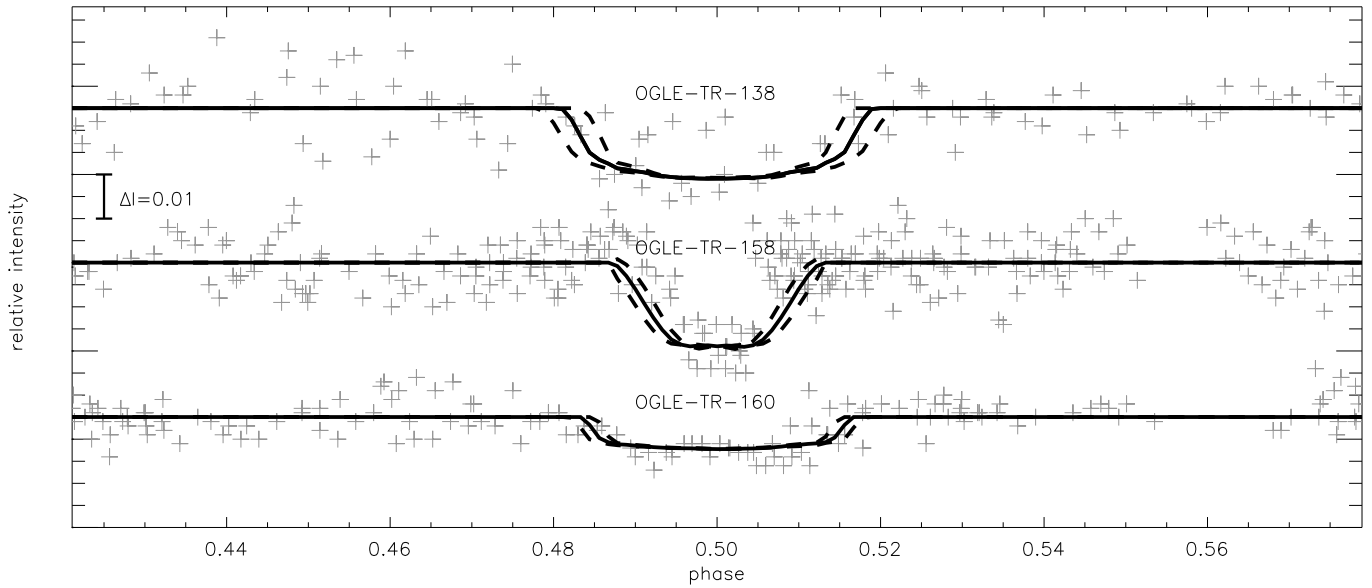


**Fig. 3.** OGLE light curves for the planetary companion candidates among our target stars with our new light curve solutions assuming a planet with one Jupiter mass and an inclination of  $90^\circ$ . Solid line: Primary and companion radii from columns 3 and 5 of Table 1, dashed lines: Lower and upper values for the radii as indicated in columns 3 and 5.

**Acknowledgements.** This paper uses observations made at the South African Astronomical Observatory (SAAO, Run No. 163), kindly supported by D. Kilkeny. S.S. acknowledges a travel grant from the Deutsche Forschungsgemeinschaft (DR-281/21-1). We acknowledge the use of the Nightfall program for the light curve synthesis of eclipsing binaries written by Rainer Wichmann (<http://www.lsw.uni-heidelberg.de/~rwichman/Nightfall.html>).

## References

- Bakos, G. A., Noyes, R. W., Kovacs, G. et al. 2006, *ApJ*, in press, arXiv:astro-ph/0609369
- Baraffe, I., Chabrier, G., Allard, F., & Hauschildt, P. H. 1998, *A&A*, 337, 403
- Baraffe, I., Chabrier, G., Allard, F., & Hauschildt, P. H. 2002, *A&A*, 382, 563
- Beaulieu, J.-P., Bennett, D. P., Fouque, P., et al. 2006, *Nature*, 439, 437
- Biller, B. A., Kasper, M., Close, L. M., Brandner, W., & Kellner, S. 2006, *ApJ*, 641, L141
- Bond, I. A., Udalski A., Jaroszynski M., et al. 2004, *ApJ*, 606, L155
- Bouchy, F., Udry, S., Mayor, M., et al. 2005, *A&A*, 444, L15
- Chabrier, G., Baraffe, I., Allard, F., & Hauschildt, P. H. 2000, *ApJ* 542, 464
- Charbonneau, D., Brown, T. M., Noyes, R. W., & Gilliland, R. L. 2002, *ApJ*, 568, 377
- Charbonneau, D., Allen, L. E., Megeath, et al. 2005, *ApJ*, 626, 523
- Charbonnel, C., Däppen, W., Schaerer, D., et al. 1999, *A&AS*, 135, 405
- Chauvin, G., Lagrange, A.-M., Dumas, C., et al. 2004, *A&A*, 425, L29
- Chauvin, G., Lagrange, A.-M., Dumas, C., et al. 2005, *A&A*, 438, L25
- Chauvin, G., Lagrange, A.-M., Zuckerman, et al. 2005, *A&A*, 438, L29
- Collier Cameron A., Bouchy F., Hebrard G., et al., 2006, *MNRAS*, in press, arXiv:astro-ph/0609688
- Cox, A.N. ed. 2000, *Allen's Astrophysical Quantities*, Fourth Edition, Springer-Verlag, p. 389
- Deming, D., Seager, S., Richardson, L. J. & Harrington, J. 2005, *Nature*, 434, 740
- Dreizler, S., Rauch, T., et al. 2002, *A&A*, 391, L17
- Gallardo, J., Minniti, D., Valls-Gabaud, D., & Rejkuba, M. 2005, *A&A*, 431, 707
- Gillon, M., Courbin, F., Magain, P., & Borguet, B. 2005, *A&A*, 442, 731
- Gould, A., Udalski, A., An, D., et al. 2006, *ApJ*, 644, L37
- Heinze, A. N., & Hinz, P. M. 2005, *AJ*, 130, 1929
- Kervella, P., Thévenin, F., Di Folco, E., & Ségransan, D. 2004, *A&A*, 426, 297
- Konacki, M., Torres, G., Sasselov, D. D., & Jha, S. 2003b, *ApJ*, 597, 1076
- Mayor, M., Queloz, D. 1995, *Nature*, 378, 355
- McCullough, P. R., Stys, J. E., Valenti, J. A., et al. 2006, *ApJ*, 648, 1228
- Neuhäuser, R., Guenther, E. W., Wuchterl, et al. 2005, *A&A*, 435, L13
- O'Donovan, F. T., Charbonneau, D., Mandushev, G. et al. 2006, *ApJ*, in press, arXiv:astro-ph/0609335
- Pont, F., Melo, C. H. F., Bouchy, F., et al. 2005a, *A&A*, 433, L21
- Pont, F., Bouchy, F., Melo, C., et al. 2005b, *A&A*, 438, 1123
- Ramírez, I., Meléndez, J., 2005, *ApJ*, 626, 465
- Santos, N. C., Bouchy F., Mayor M., et al. 2004, *A&A*, 426, L19
- Sato, B., Fischer, D. A., Henry, G. W., et al. 2005, *ApJ*, 633, 465
- Schaller, G., Schaerer, D., Meynet, G., & Maeder, A. 1992, *A&AS*, 96, 269
- Schneider, J. 2001, *Encyclopedia of Astron. & Astrophys.*, ed. P. Murdin, IoP Publishing, Bristol and Nature Publishing Group, London
- Seager, S. & Mallén-Ornelas, G. 2003, *ApJ*, 585, 1038
- Silva, D.R., Cornwell, M.E. 1992, *ApJS*, 81, 865
- Tingley, B. Sackett, P. D. 2005, *ApJ*, 627, 1011
- Udalski, A., Paczynski, B., Zebun, K., et al. 2002a, *Acta Astronomica*, 52, 1
- Udalski, A., Zebun, K., Szymanski, M., et al. 2002b, *Acta Astronomica*, 52, 115
- Udalski, A., Szweczyk, O., Zebun, K., et al. 2002c, *Acta Astronomica*, 52, 317
- Udalski, A., Pietrzynski, G., Szymanski, M., et al. 2003, *Acta Astronomica*, 53, 133
- Udalski, A., Szymanski, M. K., et al. 2004, *Acta Astronomica*, 54, 313
- Udalski, A., Jaroszyński, M., Paczyński, B., et al. 2005, *ApJ*, 628, L109
- Vidal-Madjar, A., Désert, J.-M., Lecavelier des Etangs, et al. 2004, *ApJ*, 604, L69
- Wolszczan, A., Frail, D.A. 1992, *Nature*, 355, 145

## List of Objects

- ‘OGLE-TR-149’ on page 5
- ‘OGLE-TR-153’ on page 5
- ‘OGLE-TR-167’ on page 5
- ‘OGLE-TR-172’ on page 5
- ‘OGLE-TR-82’ on page 5
- ‘OGLE-TR-139’ on page 5
- ‘OGLE-TR-142’ on page 5
- ‘OGLE-TR-163’ on page 5
- ‘OGLE-TR-139’ on page 5
- ‘OGLE-TR-142’ on page 5
- ‘OGLE-TR-82’ on page 5
- ‘OGLE-TR-163’ on page 5
- ‘OGLE-TR-82’ on page 5
- ‘OGLE-TR-138’ on page 5
- ‘OGLE-TR-158’ on page 5
- ‘OGLE-TR-160’ on page 5
- ‘OGLE-TR-163’ on page 5